Doppler-free spectroscopy of an atomic beam probed in traveling-wave fields

Jin-Lu Wen (温金录) [1] Jia-Dong Tang (唐家栋),[2] Jun-Feng Dong (董俊峰) [1] Xiao-Jiao Du (杜小娇),[3]
Shui-Ming Hu (胡水明),[1,2,*] and Y. R. Sun (孙羽) [3,†]

[1]*Department of Chemical Physics, University of Science and Technology of China, Hefei 230026, China*
[2]*Hefei National Research Center of Physical Sciences at the Microscale, University of Science and Technology of China, Hefei 230026, China*
[3]*Institute of Advanced Science Facilities, Shenzhen 518107, China*

We propose a method to probe the precision spectroscopy of an atomic beam using traveling-wave laser beams. The method is demonstrated by measuring the $2\,^3S - 2\,^3P$ transition in a slow helium atomic beam. The first-order Doppler shift could be effectively suppressed by up to three orders of magnitude compared to that induced by the probing light beam. This method avoids using a standing-wave field when probing the spectra, and consequently, it reduces the laser power dependence and eliminates the modulation due to the standing-wave field. Preliminary measurements of the $2\,^3S - 2\,^3P$ transition of ^{4}He indicate that the uncertainty could be reduced to the sub-kHz level.

I. INTRODUCTION

Precision spectroscopy based on atomic beams has achieved a number of remarkable advances in the last few decades. The spectroscopies of atomic hydrogen [1–6] and helium [7–11], inherited with the advantage of their simple structures and high accuracy in theoretical calculations, are excellent platforms for testing quantum electrodynamics [9,10,12–14], determining fundamental physical constants and nuclear structure parameters [1–3,15–17], and even searching for new physics [18–21]. In these precision measurements, it is critical to reduce the Doppler effect, which comes from imperfect alignments of the optical probing beam with respect to the atomic beam, resulting in spectral broadening and frequency shifting. To accurately determine the transition center frequency, usually, two counterpropagating laser beams are used to probe the spectrum simultaneously to eliminate the first-order Doppler shift.

Standard methods used to align the optical beams include the prism reflection method [22,23], the cat's eye method [24], the interferometric method [25], and the active fiber-based retroreflector (AFR) method [26,27]. Among them, both the cat's eye method and the AFR method reported that the deviation angle ξ between two counterpropagating laser beams could be adjusted to below 10 μrad. However, both of these methods require the use of a standing-wave field, which is realized by reflecting the incident laser beam, and there are challenges: (1) It requires the angle between the laser beam and the atomic beam to be sufficiently close to $\pi/2$, usually the deviation should be less than 1 mrad [26]. However, it could be challenging when the atomic beam itself has a considerable divergence angle. Particular efforts are needed to precisely evaluate the angle with optical [26] or spectroscopic [8] methods. (2) Since the spectral signal is

proportional to the light intensity, differences in parameters of the two counterpropagating light beams, such as light intensity, polarization, and wavefront properties, may lead to systematic deviations in the result [27]. (3) The standing-wave field may induce a detectable laser-cooling effect on the atomic beam [28]. When the probing laser is red-detuned, it will slightly converge the atoms, and when the laser is blue-detuned, it will have a diverging effect on the atoms. Consequently, the profile of the observed spectrum would be distorted by the standing-wave field [8,24,28]. (4) In addition, since the first-order Doppler shift cannot be derived directly from spectra probed with standing-wave fields, more efforts are required in the assessment of the residual Doppler shift.

Here we propose a scheme for precision spectroscopy in atomic beams using sequential counterpropagating traveling-wave optical pulses (SCTOP). The method is demonstrated by measuring the $2\,^3S - 2\,^3P$ transition of helium in an atomic beam. The transition has been extensively studied [8,9,24,29,30] to determine the fine-structure constant and charge radii of the helium nuclei. The results show that this method can effectively suppress the first-order Doppler effect and reduce systematic uncertainty.

II. EXPERIMENTAL

The optical layout is shown in Fig. 1. The probing laser beam is divided into two beams, labeled as Probe 1 and Probe 2, and coupled into two 8-m-long polarization-maintaining fibers. Then, each beam is focused by an aspheric lens with a focal length of 8 mm, and the distance between the lens and the fiber end is adjusted to locate the beam waist near the atomic beam. Both laser beam radii crossing the atomic beam are about 1.0 mm, which is measured by a beam quality analyzer. An acoustic-optic modulator (AOM) is placed in the path of each laser beam, and the laser beam polarization is purified by a Glan-Taylor (GT) prism. The light intensity is monitored and a feedback servo is applied to adjust the intensity of the rf signal driving the AOM. In this way, the

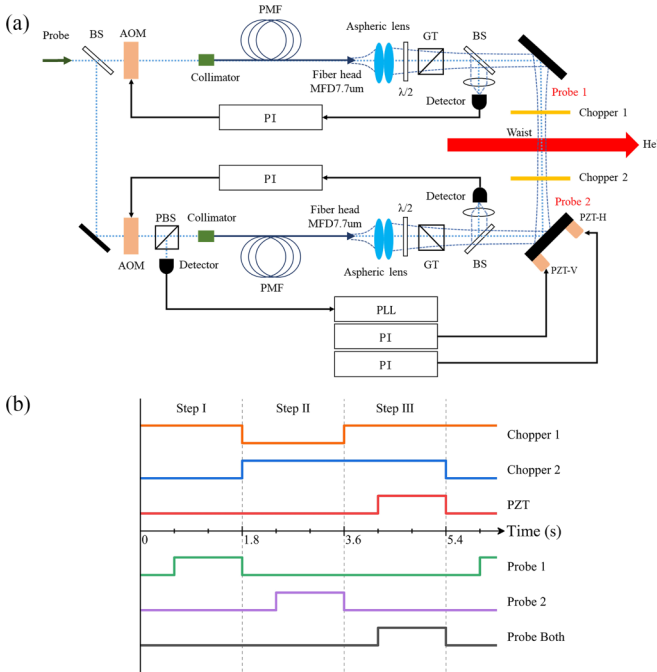*smhu@ustc.edu.cn
†sunyu@mail.iasf.ac.cn

FIG. 1. (a) Optical layout and (b) the timing sequence applied in the SCTOP measurement. BS: beam splitter; PBS: polarization beam splitter; PMF: polarization maintaining fiber; GT: Glan-Taylor prism; PZT: piezoelectric transducer; PLL: phase-lock loop; PI: proportional-integral controller.

laser power drift is reduced to be below 0.1%, and the polarization is purified to be better than 1000:1 before interacting with the atomic beam. In the experiment, the laser power can be adjusted to a preset value by rotating the $\lambda/2$ waveplate before the GT prism. The overlap between the two probing beams is accomplished by adjusting the optical path of Probe 2 to couple the Probe 1 beam into the fiber of Probe 2. The typical coupling efficiency is around 85% in the experiment.

Spectroscopy measurements were carried out with traveling-wave probing beams instead of a standing-wave field. However, we still need a precise overlap control of the counterpropagating probing beams, Probe 1 and Probe 2. We applied a modulation on the mirror mount equipped with piezo actuators (PZT-H and PZT-V shown in Fig. 1), detected the change of the light intensity coupled into the optical fiber Probe 2 from Probe 1, and demodulated the signal with a lock-in amplifier (SR830, SRS). The resulting error signal was digitized by an acquisition card (PCI-6259, NI). Using a digital proportional-integral algorithm, we obtained feedback signals and sent them to PZT-H and PZT-V. As a result, light intensity from Probe 1 coupled into the optical fiber of Probe 2 could be maintained at the maximum when the servos are closed. In the measurement, we applied a timing sequence to control the servo and record the spectrum, as shown in Fig. 1(b). Each measurement cycle applies sequential counterpropagating traveling-wave optical pulses (SCTOP), which involves three steps, each about 1.8 s. In the first step, chopper 1 in the optical path of Probe 1 was open and chopper 2 in the optical path of Probe 2 was closed. It took about 600 ms to lock the laser frequency and power, 200 ms to stabilize the system, and then 1 s to record the spectrum

with only Probe 1. In the second step, chopper 1 was closed, chopper 2 was open, and a spectrum with only Probe 2 was recorded. Finally, both choppers were open, and the feedback servos controlling PZT-H and PZT-V were turned on, which changed the voltages on PZTs and optimized the overlap between Probe 1 and Probe 2. Notice that during the first two steps, the signal of backward light intensity was still recorded, but the voltages applied to the PZTs remained without change. If needed, we can also measure the spectrum with both Probe 1 and Probe 2 (standing-wave mode) in the third step.

To avoid interference between the error signals demodulated for the vertical and horizontal dimensions, the modulation frequencies of the two locking servos were set as 290 Hz and 310 Hz, respectively. The output voltages of the digital proportional-integral-differential (PID) servo were kept within ± 1V in the experiment, to ensure that both PZTs worked in their linear range. Since the longitudinal velocity of the atomic beam [31] is much larger than its transverse velocity, the frequency shifts due to the drift of the pointing angle of the PZT-driven mirrors are negligible. The drift of the horizontal locking voltage was 3 mV and the resulting Doppler shift was estimated to be below 10 Hz. However, the error signal's offset may affect the feedback result more significantly. In the experiment, we periodically turn off the two choppers to record the zero signal without light to correct the offset. Both choppers were placed slightly off the normal angle to the laser beam to avoid the reflection of light from the chopper blades.

The spectral scanning method is similar to that used in our previous work [8], and we just give a brief description here. Before entering the probing region, metastable helium atoms were populated in $m = \pm 1$ states by optical pumping. In the probing region, the geomagnetic field was shielded by a three-layer magnetic shield, and a magnetic field was actively applied through a cosine coil. When scanning the probing laser frequency, two peaks corresponding to $m = \pm 1$ states were recorded, and the $2\,^3S - 2\,^3P$ transition center frequency was derived as the average of these two peak centers.

III. RESULTS

We measured spectra of the $2\,^3S_1 - 2\,^3P_0$ transition under the same experimental conditions using two traveling-wave beams, and the results are shown as blue and green triangles in Fig. 2(a). Note that only the $m = +1$ spectra are shown here. Each spectrum was fitted with a single Lorentz function, and the center position is indicated as the blue or green line. Since the incident lights were not perfectly perpendicular to the atomic beam, there is a frequency shift between the two peaks. The red line marks the average of the two positions. Note that if we fit the overlapped spectra with a single Lorentzian function, the line center derived from the fit will shift from the averaged position given above, since the heights of the two spectra are different.

Figure 2(b) shows the SCTOP results obtained with laser beams under different incident angles. The horizontal axis uses half of the difference between the two centers obtained with counterpropagating laser beams, which corresponds to the first-order Doppler frequency shift, being proportional to
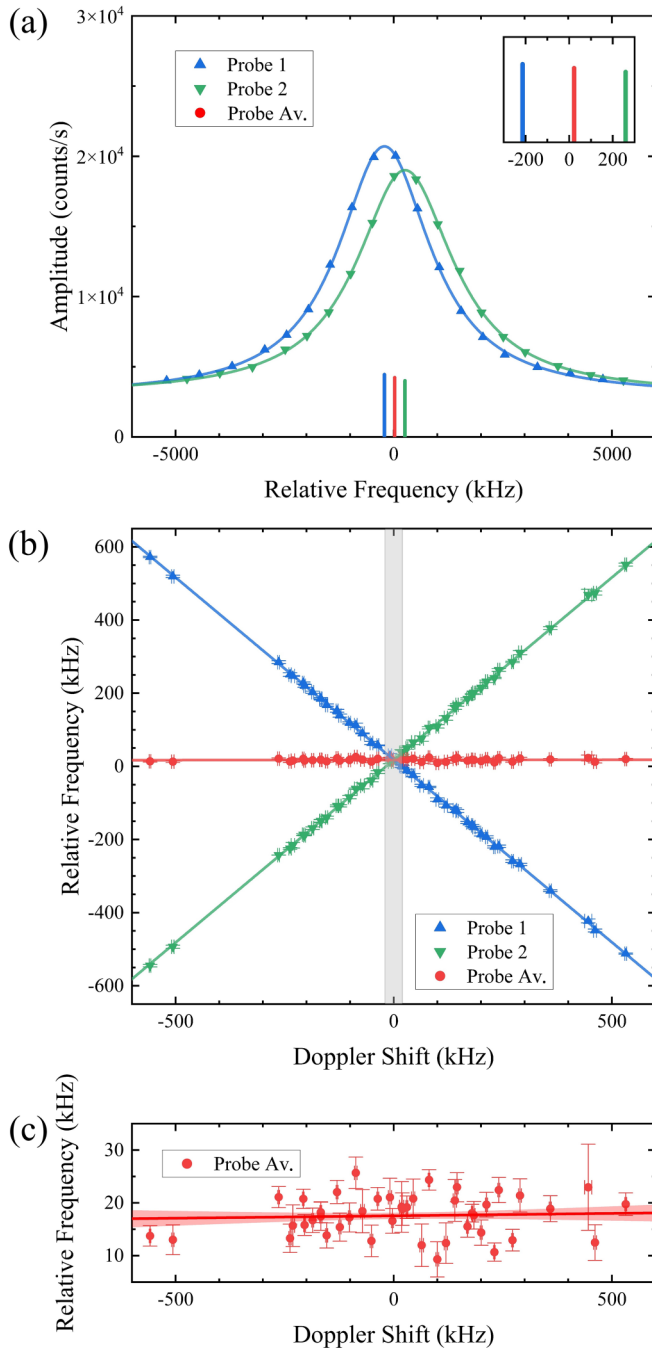
FIG. 2. (a) Spectra and centers of the $m = +1$ line obtained with two counterpropagating traveling-wave probing laser beams. The red line represents the average of the two centers. (b) Line centers from respective laser beams (blue and green) and their average values (red) probed by laser beams with different incident angles. The horizontal axis is half of the difference between the line centers obtained by Probe 1 and Probe 2, corresponding to the first-order Doppler shift. (c) Close-up of the averaged line centers shown in (b). The red shadow indicates the 1σ range of a linear fit of the data. At the limit of zero Doppler shift, the uncertainty of the averaged value is 0.6 kHz.

the laser incident angle deviating from $\pi/2$. Each red point presents the average value of a pair of results (blue point and green point) obtained under the same incident angle. A linear
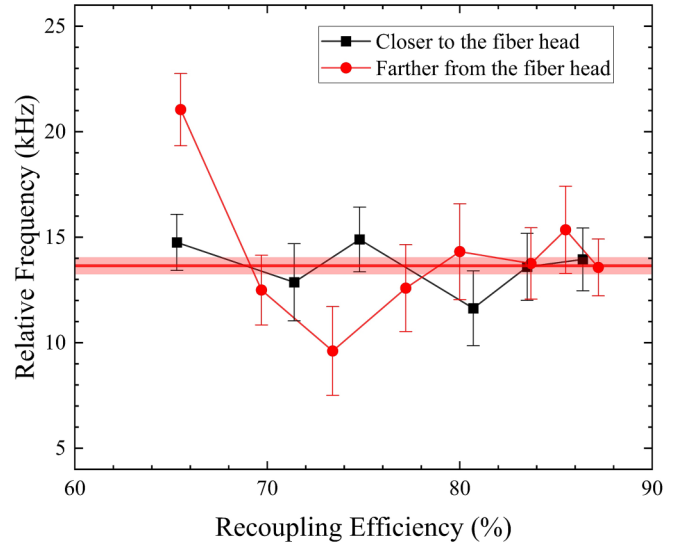

FIG. 3. The coupling efficiency and the relative frequency shift were obtained under different experimental conditions. Black squares and red circles represent data obtained by moving a lens close to the Probe 2 fiber head (black) and the other one far from the fiber head (red). The red shading region represents the 1σ range of all results obtained with efficiency above 80%.

fit of all the red points is shown in Fig. 2(c). The light red shadow represents the 1σ range of the linear fit. The result from the linear fit agrees well with the simple average value of all the data in the whole range, which has a statistical uncertainty of 0.6 kHz. Note that the maximum Doppler shift reaches 500 kHz, corresponding to an incident angle up to 3.5 mrad. It means that the Doppler shift has been reduced by almost three orders of magnitude in this SCTOP method. In conventional measurements with standing-wave fields, it is necessary to align the incident light angle as close to $\pi/2$ as one can. In our previous standing-wave field experiment [8], the range allowed for the measurement is indicated as the gray shadow region on Fig. 2(b), and the corresponding Doppler shift is within ± 20 kHz. We can see that aligning the incident probing laser beam could be much easier in present measurements, which considerably reduces the experimental difficulty.

As mentioned above, the SCTOP measurement method reduces the requirement in the control of the incident angle of the laser beam, but it is still critical to have excellent control of the overlap of the laser beam. The above-mentioned locking method ensures the overlap of the counterpropagating laser beams. However, the waist position and wavefront properties of the two beams may also affect the results. To evaluate the impact of this effect, we changed the position of the lens with a translation stage and measured the coupling efficiency of the reflected light controlled by the automatic feedback loop. We found that different lens positions led to different optimized coupling efficiencies. Spectroscopy measurements were carried out under these conditions, and the results are shown in Fig. 3. It can be seen that when the coupling efficiency decreases to below 70%, there could be observable deviations among the results obtained under different conditions. When the coupling efficiency reaches 80% and above, the deviation
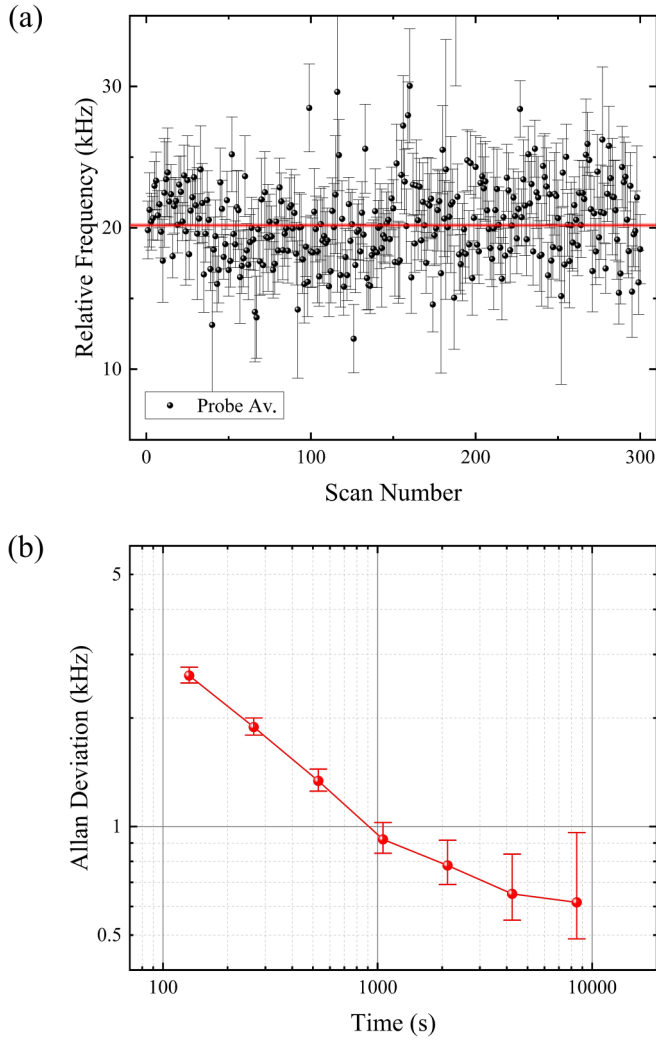
(a)

(b)

FIG. 4. (a) Center frequency of the observed $2\,^3S - 2\,^3P$ transition of ^{4}He. Each data point corresponds to an average of two spectra of Probe 1 and Probe 2. The incident probe laser angle was -120 μrad. (b) Allan deviation of the data shown in (a).
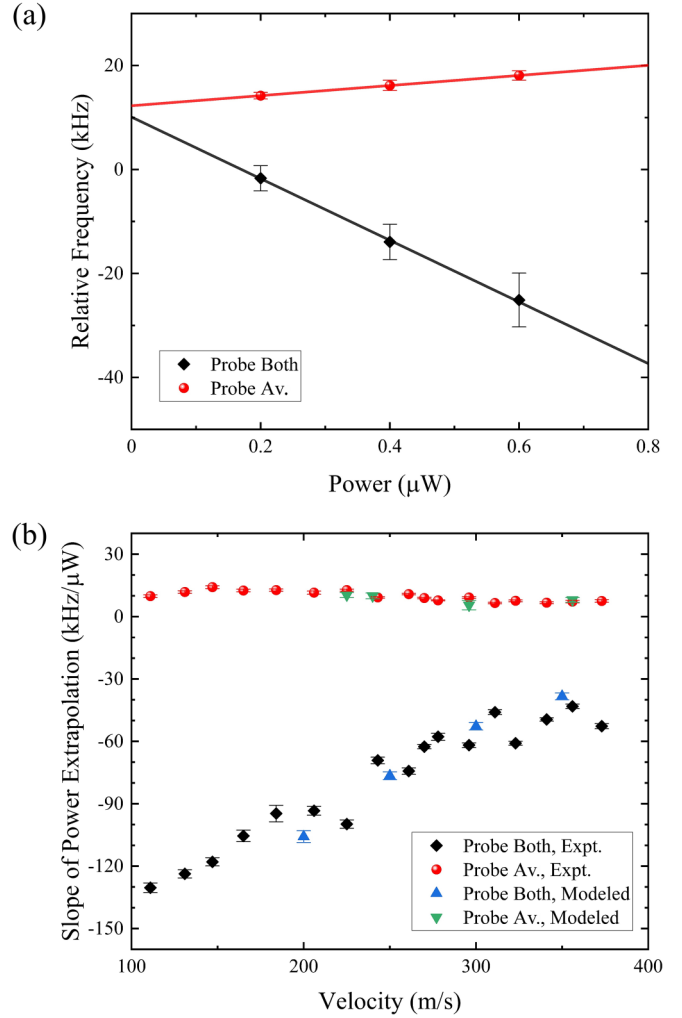
(a)

(b)

FIG. 5. (a) The probe-laser power dependence of the center frequency of the spectrum obtained with the helium atomic velocity of 250 m/s. Red circles and black squares present data obtained with the traveling-wave method and the standing-wave method, respectively. (b) The power-dependence coefficients obtained with two methods under different atomic velocities. Green and blue triangles show the simulation results of the Monte Carlo wave-function approach.

is within the experimental uncertainty. In this work, we readjusted the optical alignment every day to ensure that the coupling efficiency was kept above 85%.

Under the above conditions, we can continuously measure for hours. As an example, center frequencies (after averaging those from Probe 1 and Probe 2) obtained in a measurement of about 11 h are shown in Fig. 4. Each data point in Fig. 4(a) corresponds to the result of a single spectrum collected within 130 s, and the Allan deviation is shown in Fig. 4(b). We can see that the statistical uncertainty of the measurement is less than 1 kHz within an average time of about 1000 s.

It has been found [8] that the observed center of the $2\,^3S - 2\,^3P$ transition has a significant dependence on the power of the standing-wave probing laser. Extrapolation to the zero-power limit was applied to derive the line center, but there could be a systematic shift. Figure 5(a) shows transition frequencies obtained by the traveling-wave and standing-wave methods using the present apparatus under different laser powers. The velocity of helium atoms was measured [31] to

be 250 ± 5 m/s. It can be seen that the power dependence is much less in the results from the traveling-wave method. The coefficient decreases from 59 kHz/μW in the standing-wave method to 9.7 kHz/μW in the traveling-wave method. We did similar measurements under different atomic velocities, and the experimental power-dependent coefficients are shown in Fig. 5(b). We can see that coefficients derived from standing-wave measurements are considerably larger than those from traveling-wave measurements, and the absolute value increases at lower atomic velocities, being consistent with the results we observed before [31]. However, the coefficient obtained in traveling-wave measurements is rather small, and the value almost remains unchanged when the atomic velocity changes in the range of 100–400 m/s. This result indicates that the systematic uncertainty due to the power dependence could be much less in the traveling-wave measurements.

We also use the Monte Carlo wave-function approach to simulate the power-dependent coefficients in both traveling-wave and standing-wave methods. The method is similar to that given in Ref. [28], and the results are shown in Fig. 5(b) with blue and green triangles, agreeing well with the experimental data. A possible mechanism could be as follows. In a standing-wave field, due to the presence of laser beams in both directions, an atom may have a change in its momentum by $-2\hbar k$, 0, or $2\hbar k$, after a cycle of stimulated absorption and stimulated emission. Since the atom could go through many cycles before the spontaneous decay to the $m = 0$ level and no longer interacts with the laser field, the momentum change could be detectable under a high-power standing-wave field. Consequently, the frequency shift due to the change of the atomic velocity along the laser beam would be significant. As for that in a traveling-wave field, the momentum of the atom does not change after a cycle of stimulated absorption and emission. Therefore, the power-dependent effect in a traveling-wave field could be much less than that in a standing-wave field.

Due to the angular deviation between the two counterpropagating laser beams and spherical aberration, there may be a residual first-order Doppler shift in the resulting center frequency, which can be expressed as

$$\Delta\nu_D = \frac{1}{2}\left(\frac{\vec{k}_1 \cdot \vec{v}}{2\pi} + \frac{\vec{k}_2 \cdot \vec{v}}{2\pi}\right) = \nu_0 \frac{v}{2c}[\cos(\alpha + \xi) - \cos(\alpha)]. \tag{1}$$

Here $\vec{k}_1$ and $\vec{k}_2$ are wave vectors of the counterpropagating laser beams, $\vec{v}$ is the atomic velocity, ν_0 is the transition center frequency to be determined, c is the speed of light, α is the angle between the laser beam and the atomic beam, and ξ is the angle deviation between the two opposite laser beams. Considering α is close to $\pi/2$, and ξ is very small ($\ll 1$ mrad), the equation could be simplified to

$$\Delta\nu_D \simeq \nu_0 \frac{v}{c}\frac{\xi}{2}. \tag{2}$$

With a ξ value of 1 μrad and an atomic velocity of 100 m/s, the corresponding residual Doppler shift is 46 Hz. To evaluate the residual Doppler shift, we measured the $2\,^3S_1 - 2\,^3P_0$ transition of ^{4}He at different atomic speeds. The results are shown in Fig. 6. If we apply a linear fit of the data, we obtain a slope of $-0.0036(32)$ kHz m^{-1} s, corresponding to an angle of $\xi \approx 7.8 \pm 6.9$ μrad according to Eq. 2. The first Doppler shift could be estimated with the intercept of the linear fit shown in the figure, which is 0.89 kHz. The total measurement time at one velocity is only about 1/3 of that used in our previous work [8] in a helium beam with much higher velocities, but the statistical uncertainty is much lower. Note that the measurement of data shown in Fig. 6 spreads in a period of about 5 months, indicating an excellent consistency among the results. In particular, the systematic uncertainty due to the first-order Doppler shift, which is the leading uncertainty in the previous result [8], is confirmed to be reduced in this work. Future measurements with sub-kHz accuracy may help to resolve the discrepancy between previous measurements [8,29].
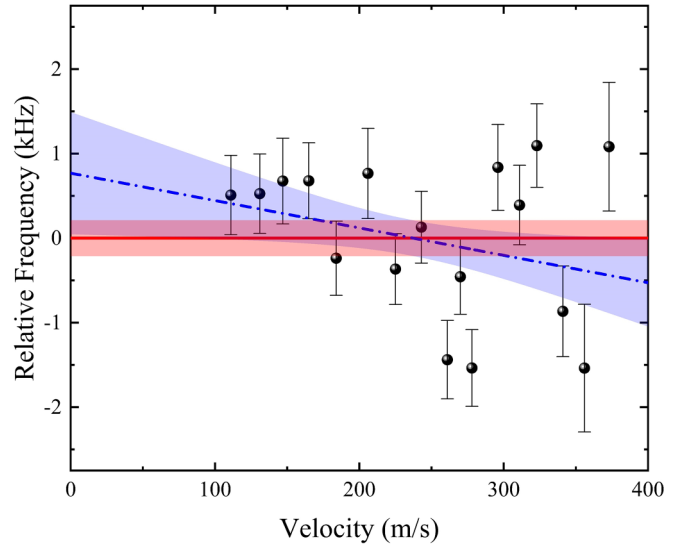

FIG. 6. Relative center frequencies obtained from spectra recorded under different atomic velocities of ^{4}He. The red belt shows the mean value and its uncertainty ($\sigma = 0.22$ kHz). The dashed blue line is the linear fit of the data and the blue shading represents the deviation range of the linear fit, which has an intercept of $+0.89(81)$ kHz and a slope of $-0.0036(32)$ kHz m^{-1} s.

IV. CONCLUSION

We demonstrate an approach to eliminate the Doppler shift in precision spectroscopy experiments, using traveling-wave probing laser beams instead of a standing-wave field. Spectra are recorded alternately using the counterpropagating probing beams, and the center frequencies are averaged to eliminate the first-order Doppler shift. Two probing laser beams are aligned with the optical fiber feedback method alternatively during the measurement. The residual Doppler shift could be eliminated even when the initial probing laser beam has a significant deviation from the perfect alignment. Measurements of the $2\,^3S - 2\,^3P$ transition of helium atoms show that this method can reduce the Doppler shift to below 0.89 kHz, corresponding to an equivalent alignment better than 10 μrad. This method can also effectively reduce the laser power-dependent effect, and eliminate the modulation and interference caused by the standing-wave field [32]. Therefore, it will considerably reduce systematic uncertainty. The method will be applied in our future measurement of the ^{4}He - ^{3}He isotope shift. Combined with the latest theoretical advances [8,33], we expect a new determination of the nuclear charge radius of the helium nucleus. This method could also be widely applied in various precision spectroscopy experiments based on atomic or molecular beams.

ACKNOWLEDGMENTS

[1] A. Grinin, A. Matveev, D. C. Yost, L. Maisenbacher, V. Wirthl, R. Pohl, T. W. Hänsch, and T. Udem, Two-photon frequency comb spectroscopy of atomic hydrogen, Science **370**, 1061 (2020).

[2] A. D. Brandt, S. F. Cooper, C. Rasor, Z. Burkley, A. Matveev, and D. C. Yost, Measurement of the $2S_{1/2} - 8D_{5/2}$ Transition in Hydrogen, Phys. Rev. Lett. **128**, 023001 (2022).

[3] N. Bezginov, T. Valdez, M. Horbatsch, A. Marsman, A. C. Vutha, and E. A. Hessels, A measurement of the atomic hydrogen Lamb shift and the proton charge radius, Science **365**, 1007 (2019).

[4] H. Fleurbaey, S. Galtier, S. Thomas, M. Bonnaud, L. Julien, F. Biraben, F. Nez, M. Abgrall, and J. Guéna, New Measurement of the $1S - 3S$ Transition Frequency of Hydrogen: Contribution to the Proton Charge Radius Puzzle, Phys. Rev. Lett. **120**, 183001 (2018).

[5] A. Beyer, L. Maisenbacher, A. Matveev, R. Pohl, K. Khabarova, A. Grinin, T. Lamour, D. C. Yost, T. W. Hänsch, N. Kolachevsky, and T. Udem, The Rydberg constant and proton size from atomic hydrogen, Science **358**, 79 (2017).

[6] A. Matveev, C. G. Parthey, K. Predehl, J. Alnis, A. Beyer, R. Holzwarth, T. Udem, T. Wilken, N. Kolachevsky, M. Abgrall, D. Rovera, C. Salomon, P. Laurent, G. Grosche, O. Terra, T. Legero, H. Schnatz, S. Weyers, B. Altschul, and T. W. Hänsch, Precision Measurement of the Hydrogen $1S-2S$ Frequency via a 920-km Fiber Link, Phys. Rev. Lett. **110**, 230801 (2013).

[7] J. J. Krauth, K. Schuhmann, M. A. Ahmed, F. D. Amaro, P. Amaro, F. Biraben, T.-L. Chen, D. S. Covita, A. J. Dax, M. Diepold, L. M. P. Fernandes, B. Franke, S. Galtier, A. L. Gouvea, J. Götzfried, T. Graf, T. W. Hänsch, J. Hartmann, M. Hildebrandt, P. Indelicato *et al.*, Measuring the α-particle charge radius with muonic helium-4 ions, Nature (London) **589**, 527 (2021).

[8] X. Zheng, Y. R. Sun, J.-J. Chen, W. Jiang, K. Pachucki, and S.-M. Hu, Measurement of the Frequency of the $2\,^3S - 2\,^3P$ Transition of ^{4}He, Phys. Rev. Lett. **119**, 263002 (2017).

[9] X. Zheng, Y. R. Sun, J.-J. Chen, W. Jiang, K. Pachucki, and S.-M. Hu, Laser Spectroscopy of the Fine-Structure Splitting in the $2\,^3P_J$ Levels of ^{4}He, Phys. Rev. Lett. **118**, 063001 (2017).

[10] K. Kato, T. D. G. Skinner, and E. A. Hessels, Ultrahigh-Precision Measurement of the $n = 2$ Triplet P Fine Structure of Atomic Helium using Frequency-Offset Separated Oscillatory Fields, Phys. Rev. Lett. **121**, 143002 (2018).

[11] R. J. Rengelink, Y. van der Werf, R. P. M. J. W. Notermans, R. Jannin, K. S. E. Eikema, M. D. Hoogerland, and W. Vassen, Precision spectroscopy of helium in a magic wavelength optical dipole trap, Nat. Phys. **14**, 1132 (2018).

[12] G. Clausen, P. Jansen, S. Scheidegger, J. A. Agner, H. Schmutz, and F. Merkt, Ionization Energy of the Metastable $2\,^1S_0$ State of ^{4}He from Rydberg-Series Extrapolation, Phys. Rev. Lett. **127**, 093001 (2021).

[13] B. M. Henson, J. A. Ross, K. F. Thomas, C. N. Kuhn, D. K. Shin, S. S. Hodgman, Y.-H. Zhang, L.-Y. Tang, G. W. F. Drake, A. T. Bondy, A. G. Truscott, and K. G. H. Baldwin, Measurement of a helium tune-out frequency: An independent test of quantum electrodynamics, Science **376**, 199 (2022).

[14] K. F. Thomas, J. A. Ross, B. M. Henson, D. K. Shin, K. G. H. Baldwin, S. S. Hodgman, and A. G. Truscott, Direct Measurement of the Forbidden $2^3S_1 \rightarrow 3^3S_1$ Atomic Transition in Helium, Phys. Rev. Lett. **125**, 013002 (2020).

[15] J.-P. Karr, D. Marchand, and E. Voutier, The proton size, Nat. Rev. Phys. **2**, 601 (2020).

[16] H. Gao and M. Vanderhaeghen, The proton charge radius, Rev. Mod. Phys. **94**, 015002 (2022).

[17] E. Tiesinga, P. J. Mohr, D. B. Newell, and B. N. Taylor, CODATA recommended values of the fundamental physical constants: 2018, Rev. Mod. Phys. **93**, 025010 (2021).

[18] M. S. Safronova, D. Budker, D. DeMille, D. F. J. Kimball, A. Derevianko, and C. W. Clark, Search for new physics with atoms and molecules, Rev. Mod. Phys. **90**, 025008 (2018).

[19] F. Ficek, P. Fadeev, V. V. Flambaum, D. F. Jackson Kimball, M. G. Kozlov, Y. V. Stadnik, and D. Budker, Constraints on Exotic Spin-Dependent Interactions Between Matter and Antimatter from Antiprotonic Helium Spectroscopy, Phys. Rev. Lett. **120**, 183002 (2018).

[20] F. Ficek, D. F. J. Kimball, M. G. Kozlov, N. Leefer, S. Pustelny, and D. Budker, Constraints on exotic spin-dependent interactions between electrons from helium fine-structure spectroscopy, Phys. Rev. A **95**, 032505 (2017).

[21] C. Delaunay, C. Frugiuele, E. Fuchs, and Y. Soreq, Probing new spin-independent interactions through precision spectroscopy in atoms with few electrons, Phys. Rev. D **96**, 115002 (2017).

[22] R. C. Brown, S. Wu, J. V. Porto, C. J. Sansonetti, C. E. Simien, S. M. Brewer, J. N. Tan, and J. D. Gillaspy, Quantum interference and light polarization effects in unresolvable atomic lines: Application to a precise measurement of the ^{6,7}Li D_2 lines, Phys. Rev. A **87**, 032504 (2013).

[23] D. J. Berkeland, E. A. Hinds, and M. G. Boshier, Precise Optical Measurement of Lamb Shifts in Atomic Hydrogen, Phys. Rev. Lett. **75**, 2470 (1995).

[24] D. Shiner, R. Dixson, and P. Zhao, Precise Measurement of the Lamb Shift and Fine Structure of the $2S$ -$2P$ Transition in Triplet Helium, Phys. Rev. Lett. **72**, 1802 (1994).

[25] S. Hannemann, E. J. Salumbides, and W. Ubachs, Reducing the first-order Doppler shift in a Sagnac interferometer, Opt. Lett. **32**, 1381 (2007).

[26] A. Beyer, L. Maisenbacher, A. Matveev, R. Pohl, K. Khabarova, Y. Chang, A. Grinin, T. Lamour, T. Shi, D. C. Yost, T. Udem, T. W. Hänsch, and N. Kolachevsky, Active fiber-based retroreflector providing phase-retracing anti-parallel laser beams for precision spectroscopy, Opt. Express **24**, 17470 (2016).

[27] V. Wirthl, L. Maisenbacher, J. Weitenberg, A. Hertlein, A. Grinin, A. Matveev, R. Pohl, T. W. Hänsch, and T. Udem, Improved active fiber-based retroreflector with intensity stabilization and a polarization monitor for the near UV, Opt. Express **29**, 7024 (2021).

[28] X. Zheng, Y. R. Sun, J.-J. Chen, J.-L. Wen, and S.-M. Hu, Light-force-induced shift in laser spectroscopy of atomic helium, Phys. Rev. A **99**, 032506 (2019).

[29] P. C. Pastor, G. Giusfredi, P. DeNatale, G. Hagel, C. de Mauro, and M. Inguscio, Absolute Frequency Measurements of the $2\,^3S_1 \rightarrow 2\,^3P_{0,1,2}$ Atomic Helium Transitions around 1083 nm, Phys. Rev. Lett. **92**, 023001 (2004).

[30] T. Zelevinsky, D. Farkas, and G. Gabrielse, Precision Measurement of the Three $2\,^3P_J$ Helium Fine Structure Intervals, Phys. Rev. Lett. **95**, 203001 (2005).

[31] J.-J. Chen, Y. R. Sun, J.-L. Wen, and S.-M. Hu, Speed-adjustable atomic beam of metastable helium for precision measurement, Phys. Rev. A **101**, 053824 (2020).

[32] Y.-N. Lv, A.-W. Liu, Y. Tan, C.-L. Hu, T.-P. Hua, X.-B. Zou, Y. R. Sun, C.-L. Zou, G.-C. Guo, and S.-M. Hu, Fano-like Resonance due to Interference with Distant Transitions, Phys. Rev. Lett. **129**, 163201 (2022).

[33] V. Patkóš, V. A. Yerokhin, and K. Pachucki, Complete $\alpha^7 m$ Lamb shift of helium triplet states, Phys. Rev. A **103**, 042809 (2021).